



Cite this: DOI: 10.1039/d6na00219f

# Synthesis and electrical characterization of rhenium-doped WS<sub>2</sub> nanotubes

Abdul Ahad,<sup>ab</sup> Shigeki Saito,<sup>a</sup> Ryuji Higashinaka,<sup>a</sup> Ken Sakayauchi,<sup>a</sup> Masaharu Kikuchi,<sup>a</sup> Satoshi Kusaba,<sup>a</sup> Zheng Liu,<sup>d</sup> Yasushi Hirose,<sup>c</sup> and Kazuhiro Yanagi<sup>\*a</sup>

Tungsten disulfide nanotubes (WS<sub>2</sub>-NTs) have attracted significant interest as one-dimensional semiconducting materials for electronic and optoelectronic devices. The development of controlled doping techniques is essential for tuning their electronic properties and enhancing device performance. In this study, we performed rhenium substitution in WS<sub>2</sub>-NTs with diameters of approximately 10 nm *via* the chemical vapor transport method. The concentration of substituted Re was estimated to be approximately 1.0 at%. Structural incorporation of Re atoms into the WS<sub>2</sub>-NT lattice effectively modified the electrical properties. As a result, the Re-doped WS<sub>2</sub>-NTs exhibited electrical conductivity almost three orders of magnitude higher than that of pristine WS<sub>2</sub>-NTs. These findings reveal a strong correlation between heteroatom-induced structural modification and electrical performance, demonstrating the potential of Re doping for tailoring WS<sub>2</sub>-NTs towards advanced nanoelectronic applications.

Received 20th March 2026  
Accepted 28th May 2026

DOI: 10.1039/d6na00219f

rsc.li/nanoscale-advances

## 1. Introduction

Nanodevices utilizing one-dimensional (1D) semiconducting nanomaterials have attracted considerable attention for advanced electronic and optoelectronic applications, including field-effect transistors,<sup>1</sup> photodetectors,<sup>2</sup> nonlinear optical devices,<sup>3</sup> and nanoscale light emitters.<sup>4</sup> Miniaturized semiconductor devices based on nanostructured materials are expected to exhibit faster carrier transport, higher efficiency, and lower energy consumption.<sup>5</sup>

Tungsten disulfide nanotubes (WS<sub>2</sub>-NTs), a subclass of transition metal dichalcogenide (TMDC) NTs, are promising semiconducting nanomaterials. WS<sub>2</sub>-NTs possess chiral layered tubular structures and exhibit semiconducting behavior regardless of chirality.<sup>6</sup> Owing to their layered structure, WS<sub>2</sub>-NTs have fewer surface defects and dangling bonds than other 1D semiconductor nanomaterials, such as silicon nanowires.<sup>7</sup> Furthermore, unlike carbon NTs, WS<sub>2</sub>-NTs do not contain metallic species originating from chirality-dependent electronic structures, which is advantageous for semiconductor device applications.

For practical semiconducting applications, the development of controllable doping techniques is essential because doping plays a critical role in device architectures such as p-n junctions, field-effect transistors, logic circuits, and integrated electronic systems.<sup>8,9</sup> Regarding two-dimensional TMDC sheets, various doping strategies have been extensively investigated, including surface adsorption of dopant molecules,<sup>10</sup> substitutional doping *via* chemical exchange reactions,<sup>11</sup> defect-induced doping,<sup>12</sup> direct vapor transport,<sup>13,14</sup> and plasma or ion treatment.<sup>15</sup> However, a few studies have reported doping techniques for WS<sub>2</sub>-NTs.<sup>16,17</sup> Moreover, doping has thus far only been demonstrated for TMDC-NTs with relatively large diameters (50–100 nm).<sup>16</sup>

Recently, several groups have successfully synthesized WS<sub>2</sub>-NTs with diameters as small as 10 nm.<sup>18–20</sup> In such small-diameter NTs, strain effects significantly influence the electronic structure, including band-gap narrowing, leading to properties distinct from those of larger-diameter NTs (50–100 nm).<sup>18,21</sup> These findings raise the important question of whether conventional doping techniques can be directly applied to small-diameter WS<sub>2</sub>-NTs. The applicability and effectiveness of substitutional doping in highly curved small-diameter WS<sub>2</sub>-NTs remain largely unexplored. Thus, an investigation of doping methods for such highly curved NTs is required.

In this study, we investigated rhenium doping into ~10 nm-diameter WS<sub>2</sub>-NTs. Re doping has been widely investigated for two-dimensional TMDC flakes and sheets.<sup>22–28</sup> Although Re doping has also been reported for WS<sub>2</sub>-NTs with relatively large diameters,<sup>16,17</sup> the reported doping concentrations were limited

<sup>a</sup>Department of Physics, Tokyo Metropolitan University, Hachioji, Tokyo 192-0397, Japan. E-mail: yanagi-kazuhiro@tmu.ac.jp

<sup>b</sup>Department of Physics, Comilla University, Cumilla-3506, Bangladesh

<sup>c</sup>Department of Chemistry, Tokyo Metropolitan University, Hachioji, Tokyo 192-0397, Japan

<sup>d</sup>Muti-Material Research Institute, National Institute of Advanced Industrial Science and Technology (AIST), Nagoya 463-8560, Japan



to 0.07–0.5 at%.<sup>16</sup> It is known that Re doping can enhance the electrical conductivity of TMDC materials<sup>23–25</sup> and induce the metallic 1T phase in WS<sub>2</sub>-NTs,<sup>17</sup> suggesting that Re incorporation can strongly modify the electrical properties of WS<sub>2</sub>-NTs. In this study, a chemical vapor transport (CVT) method was employed for Re doping into small-diameter WS<sub>2</sub>-NTs, and Re doping was successfully achieved. The concentration of substituted Re was estimated to be approximately 1.0 at%, and the Re-doped WS<sub>2</sub>-NTs exhibited electrical conductivity almost three orders of magnitude higher than that of pristine WS<sub>2</sub>-NTs.

## 2. Materials and methods

### 2.1 Synthesis of Re-doped WS<sub>2</sub>-NTs

The synthesis scheme for Re-doped small-diameter WS<sub>2</sub>-NTs is illustrated in Fig. 1b. First, pristine WS<sub>2</sub>-NTs with diameters of 10–20 nm were synthesized using our previously reported chemical vapor deposition (CVD) method.<sup>19</sup> Subsequently, Re atoms were incorporated into the WS<sub>2</sub>-NT lattice *via* a chemical vapor transport (CVT) process.

To synthesize pristine WS<sub>2</sub>-NTs, W<sub>18</sub>O<sub>49</sub> nanowires (NWs) (Fig. S2) were first grown on *c*-plane sapphire substrates by a CVD process using high-purity WO<sub>2.9</sub> powder (99.99%, Thermo Scientific) as the precursor. The obtained NWs were subsequently sulfurized using sulfur lumps (99.99%, Tokyo Chemical Industry Co., Ltd) to form pristine WS<sub>2</sub>-NTs (Fig. S3).

For Re substitution into the WS<sub>2</sub>-NT lattice, a CVT process was conducted in a sealed quartz ampoule under high vacuum (approximately  $5 \times 10^{-5}$  to  $10^{-4}$  Pa) conditions (See SI section 1.1 and Fig. 1b). The ampoule was then placed in a two-zone electric furnace. ReO<sub>3</sub> powder (KOCH Chemicals Ltd) and iodine (I<sub>2</sub>, 99.99%, Sigma-Aldrich), used as the Re precursor and transport agent, respectively, were placed in the high-temperature zone, while the pristine WS<sub>2</sub>-NTs on sapphire substrates were positioned in the low-temperature zone. The temperature gradient between the two zones promoted the transport of Re species towards the WS<sub>2</sub>-NTs, enabling substitutional doping. The key synthesis parameters, including the temperature gradient (Fig. S4), reaction time (Fig. S5), and amounts of ReO<sub>3</sub> and I<sub>2</sub> (Fig. S6), were systematically optimized.

The detailed optimization procedures are described in the SI. The optimized conditions for Re-doped WS<sub>2</sub>-NT synthesis

were as follows: a temperature gradient of 700–500 °C, a reaction time of 10 h, 12 mg of ReO<sub>3</sub>, and 15 mg of I<sub>2</sub> for one sapphire substrate on which pristine WS<sub>2</sub>-NTs were synthesized by the above-described method (Fig. S1).

### 2.2 Characterizations

The morphologies of the CVD-grown W<sub>18</sub>O<sub>49</sub> NWs, pristine WS<sub>2</sub>-NTs, and Re-doped WS<sub>2</sub>-NTs were characterized using scanning electron microscopy (SEM; Phenom ProX, Thermo Fisher Scientific Inc.) and field-emission SEM (FESEM; JSM-7800F PRIME and JSM-7100F, JEOL Ltd). Transmission electron microscopy (TEM) was performed using JEM-3200FS, JEM-2100F, and JEM-2010F microscopes (JEOL Ltd). Scanning TEM (STEM) and energy-dispersive X-ray spectroscopy (EDS) analyses were conducted using a JEM-ARM200F microscope (JEOL Ltd).

The diameter distributions and interlayer spacings of the NTs, as well as the lattice fringes of the NWs, were analyzed from the TEM images using Gatan DigitalMicrograph software. Annular bright-field (ABF)-STEM imaging was performed using a JEM-ARM200F ACCELARM microscope equipped with a cold field-emission gun and double CEOS spherical aberration correctors, operated at 120 kV. Electron energy-loss spectroscopy (EELS) elemental mapping was performed using a GIF Continuum system attached to the JEM-ARM200F operated at 200 kV.

Raman spectra were acquired using a WITec Alpha300 RAS system with a 532 nm excitation laser. The device structures and NT diameters were further characterized by atomic force microscopy (AFM; Bruker).

For electrical measurements, pristine and Re-doped WS<sub>2</sub>-NTs were transferred onto Si/SiO<sub>2</sub> substrates with a 300 nm SiO<sub>2</sub> layer. Two-terminal electrodes (Ti/Au = 10 nm/100 nm) were fabricated on individual ropes of pristine and Re-doped WS<sub>2</sub>-NTs using a standard photolithography process. The channel length was 3 μm. Electrical measurements were conducted under ambient conditions at room temperature.

## 3. Results and discussion

### 3.1 Structural evaluation

First, the structure of the pristine WS<sub>2</sub>-NTs used in this study was examined. The FESEM image (Fig. S3a) shows that the pristine WS<sub>2</sub>-NTs were densely distributed and free from flake-like byproducts. The high-resolution TEM (HRTEM) image (Fig. S3b) revealed well-defined crystalline NT walls with interlayer spacings ranging from 0.62 to 0.65 nm, consistent with the layered structure of 2H-WS<sub>2</sub>-NTs. The average diameter of the WS<sub>2</sub>-NTs was  $13.24 \pm 5.08$  nm (Fig. S3c).

The Raman spectra of the pristine WS<sub>2</sub>-NTs (Fig. S3d) exhibited intense peaks at 354 and 419 cm<sup>-1</sup>, corresponding to the E<sub>2g</sub><sup>1</sup> and A<sub>1g</sub> vibrational modes of 2H-WS<sub>2</sub>, respectively.<sup>20,29</sup> These results confirm the successful synthesis of high-quality pristine WS<sub>2</sub>-NTs.

The structures of the Re-doped WS<sub>2</sub>-NTs were subsequently investigated. Fig. 2a and b show SEM and HRTEM images of the Re-doped WS<sub>2</sub>-NTs, respectively. The NTs retained

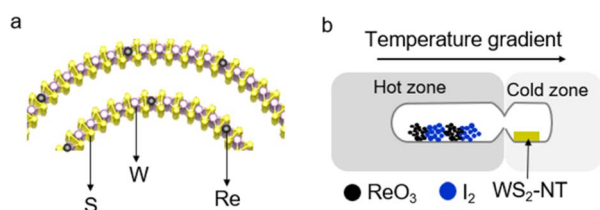


**Fig. 1** (a) Schematic illustration of Re atom substitution concept into the WS<sub>2</sub>-NT lattice. (b) Synthesis procedure of Re-doped WS<sub>2</sub>-NTs *via* the chemical vapor transport (CVT) method. In this process, I<sub>2</sub> and ReO<sub>3</sub> powders were placed in the high-temperature region, while pristine WS<sub>2</sub>-NTs were positioned in the low-temperature region. The reaction was conducted inside a high-vacuum sealed quartz ampoule.



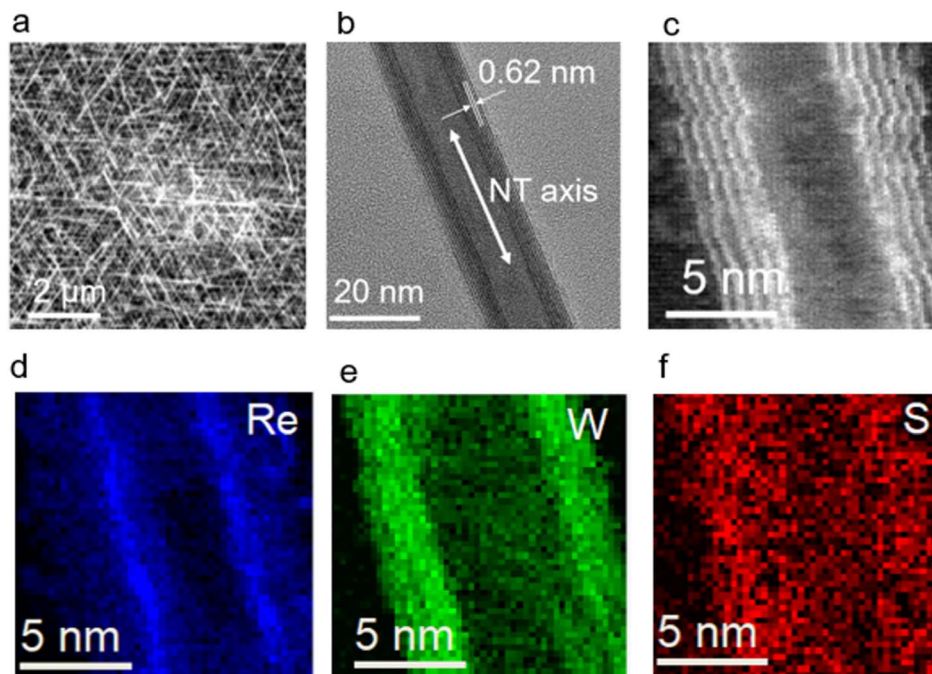


**Fig. 2** (a) SEM, (b) HRTEM, and (c) HAADF-STEM images of Re-doped WS<sub>2</sub>-NTs. The interplanar spacing varied from 0.62–0.65 nm. (d–f) EELS elemental maps of Re-doped WS<sub>2</sub>-NTs. The mapping revealed a higher concentration of Re atoms at the NT walls than within the hollow interior (d), suggesting that Re was incorporated within the layers of the WS<sub>2</sub>-NTs.

morphologies and crystalline structures comparable to those of the pristine WS<sub>2</sub>-NTs (Fig. S3a and b), indicating that the CVT doping process did not significantly damage the NT structure.

Direct identification of Re atoms within the WS<sub>2</sub>-NT lattice was challenging because of the relatively low doping concentration. In addition, Re atoms are expected to induce only minimal lattice distortion. Furthermore, the atomic number of Re is close to that of W, resulting in only weak contrast differences in the high-angle annular dark-field (HAADF)-STEM images (Fig. 2c). Nevertheless, electron energy-loss spectroscopy (EELS) mapping (Fig. 2d–f) revealed a higher Re concentration at the NT walls than in the hollow interior region (Fig. 2d), suggesting that Re atoms were incorporated into the WS<sub>2</sub>-NT layers.

### 3.2 Elemental analysis

The EDS spectra of the Re-doped WS<sub>2</sub>-NTs indicated that distinguishing W and Re signals is difficult in the M-line region because of the small energy separation and substantial overlap of their characteristic X-ray emission peaks (Fig. S7). However, distinct W and Re peaks were clearly identified in the L-line region (Fig. 3a), enabling reliable elemental analysis.

EDS measurements were performed on multiple samples and individual NTs. A histogram of Re concentrations is shown in Fig. 3b, demonstrating an average Re concentration of approximately  $1.00 \pm 0.29$  at%. These results indicate relatively uniform Re incorporation among the examined NTs.

At such doping concentrations, the possibility of Re agglomeration should be considered carefully. However, no evidence of significant Re aggregation was observed. The

HRTEM image (Fig. 2b) shows highly crystalline NT walls without detectable amorphous layers. In addition, the EELS mapping results (Fig. 2d–f) support the homogeneous incorporation of Re within the NT walls, rather than the formation of isolated Re-rich clusters. If substantial Re agglomeration had occurred, localized high-intensity Re domains would be expected in the EELS maps. Therefore, these observations suggest that Re atoms are incorporated into the WS<sub>2</sub>-NT lattice without significant agglomeration.

To further confirm Re incorporation into the WS<sub>2</sub>-NTs, the Raman spectra of WS<sub>2</sub> flakes, pristine WS<sub>2</sub>-NTs, and Re-doped WS<sub>2</sub>-NTs were measured (Fig. 3c). Several low-frequency Raman modes characteristic of WS<sub>2</sub> were observed, consistent with previous reports.<sup>30,31</sup> Because the Re concentration was relatively low, Raman features associated with ReS<sub>2</sub> were expected to be weak. Nevertheless, the Re-doped WS<sub>2</sub>-NTs exhibited an additional weak peak at approximately  $150 \text{ cm}^{-1}$ , corresponding to the in-plane  $E_g$  vibrational mode of ReS<sub>2</sub>.<sup>32</sup> These results provide additional evidence for successful Re incorporation into the WS<sub>2</sub>-NT lattice. These structural and spectroscopic analyses collectively demonstrate successful Re incorporation into small-diameter WS<sub>2</sub>-NTs while preserving the crystalline NT structure.

### 3.3 Electrical transport properties

Fig. 4a and b show AFM images of the fabricated device structures used for electrical characterization of pristine and Re-doped WS<sub>2</sub>-NTs, respectively. Typical current–voltage ( $I$ – $V$ ) characteristics of the pristine and Re-doped WS<sub>2</sub>-NT devices are presented in Fig. 4c and d. Both devices exhibited nonlinear  $I$ – $V$



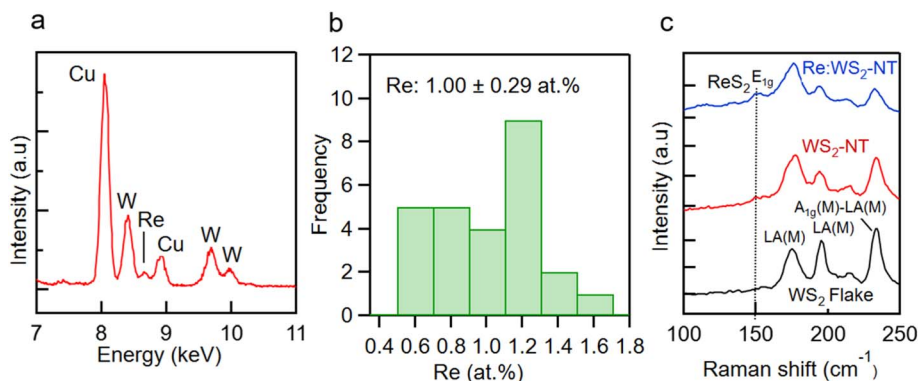


Fig. 3 (a) EDS spectrum of Re-doped WS<sub>2</sub>-NTs. (b) Histogram of Re concentrations, summarizing the EDS analysis performed on multiple NTs. (c) Raman spectra of WS<sub>2</sub> flake, pristine, and Re-doped WS<sub>2</sub>-NTs around 150 cm<sup>-1</sup>.

behavior, which is commonly observed in metal–semiconductor–metal (M–S–M) systems, owing to the formation of Schottky barriers at the metal/semiconductor interfaces.<sup>33–35</sup>

Based on the standard analytical procedure for the M–S–M model,<sup>21</sup> the electrical conductivities of pristine and Re-doped WS<sub>2</sub>-NTs were evaluated (details are provided in SI section 2). The electrical conductivity of pristine WS<sub>2</sub>-NTs was estimated to be  $2.3 \times 10^{-2} \text{ S m}^{-1}$ , whereas that of the Re-doped WS<sub>2</sub>-NTs

reached  $1.1 \times 10^1 \text{ S m}^{-1}$ , corresponding to an enhancement of almost three orders of magnitude after Re doping.

This substantial conductivity enhancement is consistent with previous reports showing that Re incorporation increases the electrical conductivity of TMDC sheets,<sup>23–25</sup> NTs, and fullerene-like nanoparticles.<sup>16</sup> Carrier densities (Table 1) were extracted from logarithmic analyses of the  $I$ – $V$  curves (Fig. S8a and b), while the Schottky barrier heights (Table 1) were

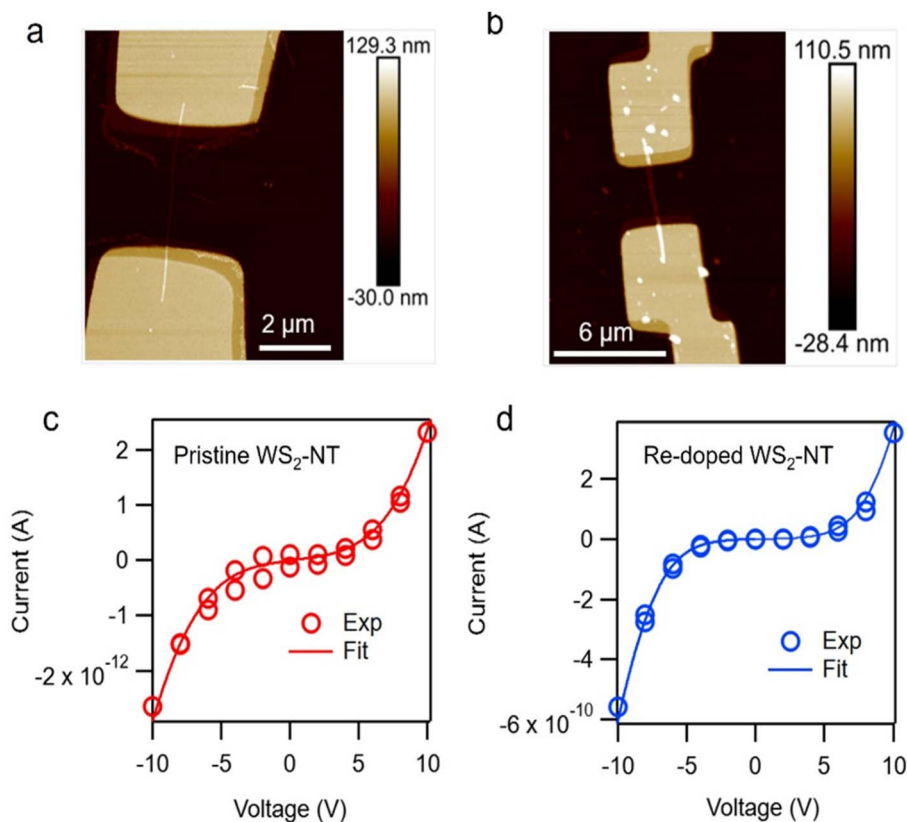


Fig. 4 AFM images of the fabricated device structures using pristine (a) and Re-doped WS<sub>2</sub>-NTs (b), with outer diameters of 19.4 nm and 11.3 nm, respectively. The channel lengths are both 3.0 μm. Current voltage ( $I$ – $V$ ) characteristics of the pristine (c) and Re-doped WS<sub>2</sub>-NTs (d) measured at room temperature. Both curves exhibit nonlinear behaviour, indicating a Schottky barrier at the interface between the Ti/Au electrodes and NTs. Experimental data (Exp) are solid circles, and fitting lines (Fit) based on a M–S–M model are solid lines.



**Table 1** Results obtained from fitting experimental  $I$ - $V$  curves of pristine and Re-doped WS<sub>2</sub>-NT devices

Parameters	Value	
	Pristine WS <sub>2</sub> -NT	Re-doped WS <sub>2</sub> -NT
Diameter, $D$ (nm)	19.4	11.3
Schottky barrier height, $\phi_b$ (eV)	0.75	0.67
Conductivity, $\sigma$ (S m <sup>-1</sup> )	$2.3 \times 10^{-2}$	$1.1 \times 10$
Carrier density, $n$ (cm <sup>-3</sup> )	$3.0 \times 10^{17}$	$4.9 \times 10^{17}$

estimated by fitting the nonlinear transport behavior using the M-S-M model.

The extracted carrier density increased moderately after Re doping. Previous studies have suggested that Re substitution shifts the chemical potential towards the conduction band,<sup>32,33</sup> which can contribute to the observed increase in carrier density. However, the relatively small increase in carrier density alone may not fully account for the almost three-orders-of-magnitude enhancement in electrical conductivity.

Previous studies have also reported that Re incorporation can induce the formation of the metallic 1T phase in WS<sub>2</sub>-based nanostructures.<sup>17</sup> The presence of such a metallic phase could additionally contribute to the enhanced electrical conductivity observed in Re-doped WS<sub>2</sub>-NTs. Although direct evidence of the 1T phase was not obtained in the present study, partial formation of the 1T phase is one possible reason for the significant conductivity enhancement.

Overall, these results demonstrate that Re incorporation strongly modifies the electrical transport properties of small-diameter WS<sub>2</sub>-NTs.

## 4. Conclusions

In this study, we demonstrated Re doping of small-diameter WS<sub>2</sub>-NTs *via* the CVT method. Effective incorporation of Re into the WS<sub>2</sub>-NT lattice was achieved, with an estimated Re concentration of approximately 1.0 at%. The structural incorporation of Re significantly modified the electrical transport properties of the WS<sub>2</sub>-NTs. As a result, the Re-doped WS<sub>2</sub>-NTs exhibited electrical conductivity almost three orders of magnitude higher than that of pristine WS<sub>2</sub>-NTs. However, since the electrical measurements were performed using a two-terminal configuration, four-terminal measurements will be necessary for a more detailed understanding of the intrinsic electrical properties. The CVT technique is not readily scalable, and thus alternative doping methods should be explored for future nanoelectronic applications of WS<sub>2</sub>-NTs. The findings of this study demonstrate that heteroatom incorporation is an effective strategy for tuning the electrical properties of small-diameter WS<sub>2</sub>-NTs. These results further highlight the potential of Re-doped WS<sub>2</sub>-NTs for future nanoelectronic applications.

## Author contributions

K. Y. proposed the project and designed the work. A. A. and R. H. performed the synthesis of Re-doped WS<sub>2</sub>-NTs. A. A.

conducted FE-SEM, EDS, and TEM measurements. A. A., K. Y. and S. K. discussed the properties. A. A., M. K., S. S. and K. S. fabricated the nanodevices and measured the AFM and analysed the electrical properties. Z. L. contributed to the STEM and EELS measurements. Y. H. supported the FE-SEM measurements. All authors participated in reviewing and editing the manuscript and approved the final version.

## Conflicts of interest

The authors declare no conflict of interest.

## Data availability

The data supporting the findings of this work are available within the article.

Supplementary information (SI): synthesis of W<sub>18</sub>O<sub>49</sub>-NWs and pristine WS<sub>2</sub>-NTs; preparation of ampoule for synthesizing Re-doped WS<sub>2</sub>-NTs (Fig. S1); FESEM, TEM and HRTEM images of W<sub>18</sub>O<sub>49</sub>-NWs (Fig. S2); structural evolution of pristine WS<sub>2</sub>-NTs (Fig. S3); temperature dependent study of Re-doped WS<sub>2</sub>-NTs (Fig. S4); reaction time dependent synthesis of Re-doped WS<sub>2</sub>-NTs (Fig. S5); effect of ReO<sub>3</sub> precursor concentration on the morphology and composition of Re-doped WS<sub>2</sub>-NTs (Fig. S6); EDS of Re-doped WS<sub>2</sub>-NTs (Fig. S7); fitting graphs for determining resistance, and carrier density (Fig. S8). See DOI: <https://doi.org/10.1039/d6na00219f>.

## Acknowledgements

K.Y. acknowledges support from JSPS KAKENHI, Grant No. JP21H05017, JP23H00259, and JP24H01200, JPJSBP120252302 and JST CREST through Grant No. JPMJCR2544, Japan, and US-JAPAN PIRE collaboration, Grant No. JPSJRP20221202, Japan, and Tokyo Metropolitan Government Advanced Research Grant Number (H31-1). K.Y. and Z.L. acknowledge support from ASPIRE project, Grant No. JPMJAP2310, Japan. R.H. acknowledges support from JSPS KAKENHI, Grant No. JP25K07228. S.S. acknowledges support from Grant No. JPMJSP2156. We would like to thank Editage (<https://www.editage.jp/>) for English language editing.

## References

- 1 Y. Huang, X. Duan, Y. Cui, L. J. Lauhon, K. H. Kim and C. M. Lieber, *Science*, 2001, **294**, 1313–1317.
- 2 S. Yip, L. Shen and J. C. Ho, *J. Semicond.*, 2019, **40**, 111602.
- 3 E. Garnett, L. Mai and P. Yang, *Chem. Rev.*, 2019, **119**, 8955–8957.
- 4 L. N. Quan, J. Kang, C. Z. Ning and P. Yang, *Chem. Rev.*, 2019, **119**, 9153–9169.
- 5 C. Zhang, S. Wang, L. Yang, Y. Liu, T. Xu, Z. Ning, A. Zak, Z. Zhang, R. Tenne and Q. Chen, *Appl. Phys. Lett.*, 2012, **100**, 243101.
- 6 G. Seifert, H. Terrones, M. Terrones, G. Jungnickel and T. Frauenheim, *Solid State Commun.*, 2000, **114**, 245–248.



- 7 C. Zhang, Z. Ning, Y. Liu, T. Xu, Y. Guo, A. Zak, Z. Zhang, S. Wang, R. Tenne and G. Chen, *Appl. Phys. Lett.*, 2012, **101**, 113112.
- 8 Y. Pan, T. Jian, P. Gu, Y. Song, Q. Wang, B. Han, Y. Ran, Z. Pan, Y. Li, W. Xu and P. Gao, *Nat. Commun.*, 2024, **15**, 9631.
- 9 H. Y. Lan, C. P. Lin, L. Liu, J. Cai, Z. Sun, P. Wu, Y. Tan, G. S. H. Yan, T. H. Hou, J. Appenzeller and Z. Chen, *Nat. Commun.*, 2025, **16**, 4160.
- 10 W. Liao, S. Zhao, F. Li, C. Wang, Y. Ge, H. Wang, S. Wang and H. Zhang, *Nanoscale Horiz.*, 2020, **5**, 787–807.
- 11 P. Luo, F. Zhuge, Q. Zhang, Y. Chen, L. Lv, Y. Huang, H. Li and T. Zhai, *Nanoscale Horiz.*, 2019, **4**, 26–51.
- 12 J. Lee, J. Heo, H. Y. Lim, J. Seo, Y. Kim, J. Kim, U. Kim, Y. Choi, S. H. Kim, Y. J. Yoon, T. j. Shin, J. Kang, S. K. Kwak, J. Y. Kim and H. Park, *ACS Nano*, 2020, **14**, 17114–17124.
- 13 G. K. Solanki, P. Pataniya, C. K. Sumesh, K. D. Patel and V. M. Pathak, *J. Cryst. Growth*, 2016, **441**, 101–106.
- 14 R. P. Patel, P. M. Pataniya, M. Patel, V. Adepu, P. Sahatiya and C. K. Sumesh, *Sens. Actuators, A*, 2023, **356**, 114339.
- 15 J. He, Y. Wen, D. Han, P. Zeng, P. Zheng, L. Zheng, W. Su, Z. Wu and Y. Zhang, *Mater. Sci. Semicond. Process.*, 2023, **158**, 107347.
- 16 L. Yadgarov, R. Rosentsveig, G. Leituss, A. Albu-Yaron, A. Moshkovich, V. Perflyev, R. Vasic, A. I. Frenkel, A. N. Enyashin, G. Seifert, L. Rapoport and R. Tenne, *Angew. Chem., Int. Ed.*, 2012, **51**, 1148–1151.
- 17 A. N. Enyashin, L. Yadgarov, L. Houben, I. Popov, M. Weidenbach, R. Tenne, M. Bar-Sadan and G. Seifert, *J. Phys. Chem. C*, 2011, **115**, 24586–24591.
- 18 M. A. Rahman, Y. Yomogida, A. Ahad, K. Ueji, M. Nagano, A. Ihara, H. Nishidome, M. Omoto, S. Saito, Y. Miyata, S. Okada, Y. Gao and K. Yanagi, *Sci. Rep.*, 2023, **13**, 16959.
- 19 A. Ahad, Y. Yomogida, M. A. Rahman, A. Ihara, Y. Miyata, Y. Hirose, K. Shinokita, K. Matsuda, Z. Liu and Y. Yanagi, *Nano Lett.*, 2024, **24**, 14286–14292.
- 20 X. H. Wang, C. C. Zheng and L. Q. and Ning, *Sci. Rep.*, 2016, **6**, 33091.
- 21 I. Milošević, B. Nikolić, E. Dobardžić, M. Damnjanović, I. Popov and G. Seifert, *Phys. Rev. B Condens. Matter.*, 2007, **76**, 233414.
- 22 L. Yadgarov, V. Petrone, R. Rosentsveig, Y. Feldman, R. Tenne and A. Senatore, *Wear*, 2013, **297**, 1103–1110.
- 23 M. A. Jenisha, S. Kavirajan, S. Harish, S. Kamalakannan, J. Archana, E. S. Kumar, N. Wakiya and M. Navaneethan, *J. Colloid Sci.*, 2024, **653**, 1150–1165.
- 24 T. Hallam, S. Monaghan, F. Gity, L. Ansari, M. Schmidt, C. Downing, C. P. Cullen, V. Nicolosi, P. K. Hurley and G. S. Duesberg, *Appl. Phys. Lett.*, 2017, **111**, 203101.
- 25 M. K. Agarwal, P. D. Patel and S. K. Gupta, *J. Cryst. Growth*, 1993, **129**, 559–562.
- 26 S. Y. Hu, M. C. Cheng, K. K. Tiong and Y. S. Huang, *J. Condens. Matter Phys.*, 2005, **17**, 3575–3583.
- 27 P. C. Yen, Y. S. Huang and K. K. Tiong, *J. Phys.: Condens. Matter*, 2004, **16**, 2171–2180.
- 28 L. Yadgarov, D. G. Stroppa, R. Rosentsveig, R. Ron, A. N. Enyashin, L. Houben and R. and Tenne, *Z. Anorg. Allg. Chem.*, 2012, **638**, 610–2616.
- 29 M. Staiger, P. Rafailov, K. Gartsman, H. Telg, M. Krause, G. Radovsky and A. Zak, *Phys. Rev. B*, 2012, **86**, 165423.
- 30 X. Huang, Y. Gao, T. Yang, W. Ren, H. M. Cheng and T. Lai, *Sci. Rep.*, 2016, **6**, 32236.
- 31 A. Berkdemir, H. R. Gutiérrez, A. R. Botello-Méndez, N. Perea-López, A. L. Elías, C. I. Chia, B. Wang, V. H. Crespi, F. López-Urías and J. C. Charlier, *Sci. Rep.*, 2013, **3**, 1755.
- 32 D. A. Chenet, B. Aslan, P. Y. Huang, C. Fan, A. M. Van Der Zande, T. F. Heinz and J. C. Hone, *Nano Lett.*, 2015, **15**, 5667–5672.
- 33 Z. Zhang, K. Yao, Y. Liu, C. Jin, X. Liang, Q. Chen and L. M. Peng, *Adv. Funct. Mater.*, 2007, **17**, 2478–2489.
- 34 C. P. Y. Zhang, H. C. Troadec, A. T. Wee and K. E. J. Goh, *Phys. Rev. Appl.*, 2020, **14**, 054027.
- 35 Z. Y. Zhang, C. H. Jin, X. L. Liang, Q. Chen and L. M. Peng, *Appl. Phys. Lett.*, 2006, **88**, 073102.

